

The linear stability of flat Stokes layers

By P. J. BLENNERHASSETT AND ANDREW P. BASSOM†

School of Mathematics, University of New South Wales, Sydney NSW 2052, Australia
P.Blennerhassett@unsw.edu.au

(Received 25 June 1999 and in revised form 12 February 2002)

The linear stability of the Stokes layer generated by an oscillating flat plate is investigated using Floquet theory. The results obtained include the behaviour of the growth rate of the disturbances, part of the corresponding neutral curve and the structure of neutrally stable disturbances. Previously unknown properties of the growth rate cause the neutral curve to have a complicated geometry: the majority of the marginal curve is defined by waves propagating relative to the basic flow and the curve is smooth in character, but for certain very narrow bands of wavenumbers it was found that stationary modes are the first to become unstable. This phenomenon has the consequence that the underlying smooth neutral curve is punctuated by thin finger-like features. The structure of the eigenfunctions showed that the neutrally stable disturbances tend to grow most rapidly just after the wall velocity passes through zero.

1. Introduction

Unsteady flows occur naturally with applications ranging from engineering to physiology. Transition to turbulence in such flows is of practical interest and there are several papers dealing with the stability of flows composed of a steady component plus an oscillatory component with zero temporal mean (Clamen & Minton 1977). In such flows a possible instability mechanism can be associated with the mean component so that the stability properties of the flow may be determined by a perturbation-type analysis, as in Hall (1975). When the oscillatory component ceases to be small compared to the mean, or in the special case when the temporal mean flow is exactly zero, the above perturbation approaches fail and the theoretical results for the stability of the flow are less definitive. Equally, the experimental information on the stability of purely oscillatory flows is somewhat inconclusive.

In an attempt to provide more precise information on the stability of oscillatory flows the work undertaken here re-considers the linear stability of the classical flat Stokes layer that is generated when an infinite rigid plate oscillates in its own plane with a velocity $U_0 \cos \omega t$. Above the plate is an infinite viscous fluid of kinematic viscosity ν and the movement of the bounding surface induces a flow which has a boundary-layer thickness $\delta \sim O(\sqrt{2\nu/\omega})$. A Reynolds number R can now be defined as

$$R = U_0 \delta / 2\nu = U_0 / \sqrt{2\nu\omega}. \quad (1.1)$$

As the basic flow is $2\pi/\omega$ -periodic in time, Floquet theory suggests that small disturbances to the flow have the form $\exp(\mu^* t) f$ plus its complex conjugate; here f

† Permanent address: School of Mathematical Sciences, University of Exeter, North Park Road, Exeter, Devon EX4 4QE, UK, drew@maths.ex.ac.uk

is a function of the independent variables which is also $2\pi/\omega$ -periodic in time and μ^* is the Floquet exponent. The first attempt to use this approach for the linear stability of the classical flat Stokes layer was made by Hall (1978, hereafter referred to as H78). His results showed no evidence of instability for R smaller than 160, as well as intervals in R where no discrete Floquet modes could be found. (Note that the Reynolds number used in H78 is twice that adopted here.) Earlier work by von Kerczek & Davis (1974) had considered the related problem in which a stationary upper boundary is placed within the fluid so the stability equations need to be solved in a finite rather than a semi-infinite domain. In their calculations the gap between the moving and stationary surfaces was chosen to be 8δ and no instability could be detected for R up to roughly 400. Many of the issues that pertain to the stability of time-periodic flows in general have been reviewed by Davis (1976) but it appears that to date all analytical and numerical studies of the linear stability of flat Stokes layers have only ever detected Floquet modes with the real part of μ^* negative. For example, Akhavan, Kamm & Shapiro (1991*b*) used direct numerical simulation to examine the linear and nonlinear stability of oscillatory flow in a channel. Their linear stability calculations were unable to find growing Floquet modes for values of R up to 500.

The main result of this paper is the prediction, based on Floquet theory, that the classical flat Stokes layer is linearly unstable for Reynolds numbers, R , greater than about 708. The wavelength of the most unstable disturbance is predicted to be approximately $2\pi\delta/0.38$. Our results also show that for R above the neutral value the growth rate of the disturbance increases almost linearly with R , at least for R up to 1000, which suggests that an inviscid instability mechanism may be present.

The comparison of the above results with existing experimental observations is not straightforward. Our theoretical predictions apply to plane Stokes layers in an unbounded fluid while most experiments are carried out in circular pipes, and the majority of numerical solutions apply to spatially bounded flows. The relationship between the linear stability of a classical flat Stokes layer and the stability of the Stokes layer in high-frequency oscillatory flow in a channel is not clear (de Souza 1998). The gaps in the spectrum reported in H78, and confirmed in our work, do not seem to have been found in channel flows and there are symmetric and antisymmetric disturbance modes possible in channel flows while there are no symmetries in the direction normal to the bounding surface for the classical Stokes layer. For the pipe experiments, high frequencies of oscillation, or large diameter pipes, are needed just to obtain a reasonable approximation to the plane Stokes layer. The high-frequency experiments of Merkli & Thomann (1975) were conducted in pipes with one end sealed, so that the spatially averaged flow is zero for all times along the length of the pipe, a property not possessed by the classical Stokes layer under consideration here. Other experimental variations are also possible: the pipe itself may oscillate, corresponding to the situation described above for the classical Stokes layer (Clamen & Minton 1977), or the oscillations in the fluid can be driven by a piston with the pipe held stationary (Akhavan, Kamm & Shapiro 1991*a*; Eckmann & Grotberg 1991; Hino, Sawamoto & Takasu 1976; Merkli & Thomann 1975). While these differences should not affect any stability predictions, they do alter the corresponding eigenfunctions and hence how any disturbances might be described. Hino *et al.* (1976) identified a number of distinct phases of flow behaviour as functions of a frequency parameter $\lambda = (\text{pipe radius})/\delta$ and their parameter R_δ (which is twice our R when λ is large). Most of the velocity traces given by Hino *et al.* are at low values of λ and hence not directly relevant to the classical Stokes layer flow. However, their results did show that at low R_δ the flow was completely laminar and that for increasing R_δ

disturbances which grew and then decayed within one cycle were possible. Their first transition, from laminar to weakly disturbed, showed the disturbance growing during the accelerating phase of the basic flow and then decaying once the velocity had passed its maximum value. Other experiments have led to different characterizations of the structure of the disturbances in the basic flow (Clarion & Pelissier 1975; Akhavan *et al.* 1991a).

Many studies, whether theoretical, numerical or experimental in nature, have suggested that disturbances in flat Stokes layers evolve in a highly non-uniform way. By this we mean that even disturbances that experience a net decay over the course of a complete period nevertheless often exhibit intervals of rapid amplification (and times of correspondingly quick decay) within the cycle. This observation has prompted the use of quasi-steady stability analysis of Stokes layer velocity profiles. The current quasi-steady theories can be divided into two broad classes: in one, there is no *a priori* asymptotic parameter and the Reynolds number is retained in the relevant version of the Orr–Sommerfeld equation (e.g. Obremski & Morkovin 1969) while in the other type R is taken to be asymptotically large. In the former case estimates of neutral conditions may be produced while using the latter approach will only lead to predictions of growth rates for the disturbances. Cowley (1987) used the asymptotically large- R technique together with a combination of high-frequency quasi-steady ideas and multiple-scales methods to demonstrate that for sufficiently large R disturbances can grow markedly over at least part of the oscillation cycle. This result is significant as it demonstrates that quasi-steadiness is the natural and self-consistent consequence of R being large. Later work by Wu & Cowley (1995) explored the weakly nonlinear development of high-frequency modes around times at which they are instantaneously neutrally stable, though a rational quasi-steady theory that describes disturbances through a complete cycle of the Stokes layer flow remains elusive. Although de Souza (1998) has demonstrated that quasi-steady theory can be a large- R asymptotic limit of Floquet theory if the mean-flow component is large enough, his argument fails in the case of the pure Stokes layer as the mean flow is zero.

While the quasi-steady, inviscid calculations of Cowley (1987) and de Souza (1998) needed to take special account of any critical layers, or other modes associated with inflection points, numerical simulations based on the governing viscous equations are relatively free from such technicalities. In the finite-Reynolds-number computations of von Kerczek & Davis (1974), in H78 and in other more recent calculations no particular measures are taken to guard against the possible existence of critical layers or inflectional instability modes. Indeed, Davis (1976) argues that at finite Reynolds numbers the inflection points in the Stokes layer are inefficient in producing instabilities as the basic flow is changing too quickly. At finite Reynolds number all that is required is an accurate approximation for the velocity field. Some calculations have been based on Galerkin or spectral methods while the work of H78 developed a formal exact solution of the governing disturbance equations.

There is a large literature dealing with various types of oscillatory flows, with much of the more recent theoretical work directed towards finding transition mechanisms which do not require a linear instability. Akhavan *et al.* (1991b) used spectral methods to solve the full Navier–Stokes equations and they showed that slowly decaying two-dimensional disturbances are highly unstable to three-dimensional modes at Reynolds numbers close to the experimentally observed transition to turbulence. Looking at other mechanisms, Vittori & Verzicco (1998) show how the oscillatory flow close to a flat but imperfect wall becomes turbulent. They demonstrated that disturbances

seen in experiments are induced by imperfections in the apparatus which in turn trigger modes which are unstable according to quasi-steady theory. When R exceeded about 275 three-dimensionality was observed and an intermittently turbulent regime evolved. We do not follow this path, but return to the quest for a linear instability.

The work presented here is a semi-analytical attempt to locate part of the linear-theory neutral stability curve for the classical Stokes layer flow on an infinite flat plate. The approach adopted is a slight reformulation of the technique used in H78, combined with more computing power than was then available to Hall. The results obtained include detailed information on the behaviour of the growth rate of disturbances to the basic flow as a function of R , part of the neutral stability curve, including a local minimum in R , and the structure of the neutrally stable perturbations. It is worth noting here that the neutral curve, shown in figures 2 and 3 below, has some novel small-scale features. However, in §4 we show that these unusual properties are the natural development, as R increases, of results originally described in H78. The remainder of this work starts with the formulation of the problem in §2 and is followed by a discussion of the numerical techniques in §3. We conclude with a description of the results and a few remarks.

2. Formulation of the numerical problem

Consider the motion induced in a semi-infinite layer of viscous fluid by a flat plate located at $y = 0$ which oscillates, in its own plane, in the x -direction with velocity $U_0 \cos \omega t$. If all lengths are scaled on $\sqrt{2\nu/\omega}$, velocities on U_0 and the non-dimensional time $\tau = \omega t$ is introduced, then in the absence of disturbances, the basic Stokes flow is given by

$$u = U_B(y, \tau) = e^{-y} \cos(\tau - y), \quad v = 0, \quad (2.1)$$

where u and v denote the flow velocities in the x - and y -directions respectively. As Squire's theorem has been extended to unsteady flows (Conrad & Criminale 1965; von Kerczek & Davis 1974) it is sufficient, for the purposes of locating the critical Reynolds number, to study the linear stability of (2.1) by imposing a disturbance of the form

$$(u, v) = (U_B, 0) + \varepsilon \left(\frac{\partial \Psi}{\partial y}, -\frac{\partial \Psi}{\partial x} \right), \quad (2.2)$$

where $\varepsilon \ll 1$ and Ψ denotes a disturbance stream function. We decompose

$$\Psi = e^{\mu\tau} e^{iax} \psi(y, \tau) + \text{complex conjugate}, \quad (2.3)$$

with $\psi(y, \tau)$ taken to be 2π -periodic with any exponential growth or decay of Ψ incorporated in μ . The associated perturbation vorticity is denoted $e^{\mu\tau} e^{iax} \zeta(y, \tau) + \text{complex conjugate}$, so the governing stream function–vorticity equations, when linearized in ε , reduces to

$$\frac{\partial \zeta}{\partial \tau} = \frac{1}{2} \left(\frac{\partial^2}{\partial y^2} - a^2 \right) \zeta - \mu \zeta - iaRU_B \zeta + iaRU_{Byy} \psi, \quad (2.4a)$$

$$\zeta = \left(\frac{\partial^2}{\partial y^2} - a^2 \right) \psi, \quad (2.4b)$$

subject to

$$\psi = \psi_y = 0 \quad \text{on} \quad y = 0; \quad \psi, \zeta \rightarrow 0 \quad \text{as} \quad y \rightarrow \infty. \quad (2.4c)$$

In this formulation $a \in \mathbb{R}$, $\mu \in \mathbb{C}$ and the imaginary part of μ , μ_i , is only determined modulo unity. Thus, for definiteness, μ_i was taken to lie in the range $-\frac{1}{2} < \mu_i \leq \frac{1}{2}$. However, the governing equations also have the property that if $\mu, \zeta(y, \tau)$ is a solution, then so is $\tilde{\mu}, \zeta(y, \tau + \pi)$ and hence left and right propagating waves with the same growth rate are possible. In consequence, the range for μ_i could be restricted further and it was only necessary to examine the interval $0 \leq \mu_i \leq \frac{1}{2}$.

The system (2.4) was analysed following the procedure given in H78. The unknowns are decomposed into harmonics $(\psi, \zeta) = \sum_{n=-\infty}^{\infty} (\psi_n(y), \zeta_n(y)) e^{in\tau}$, so that equating coefficients of the harmonics in (2.4) results in the infinite system of ordinary differential equations

$$\left(\frac{\partial^2}{\partial y^2} - a^2 - 2\mu - 2in\right) \zeta_n = iaR[(\zeta_{n-1} - 2i\psi_{n-1}) e^{-(1+i)y} + (\zeta_{n+1} + 2i\psi_{n+1}) e^{-(1-i)y}], \tag{2.5a}$$

$$\left(\frac{\partial^2}{\partial y^2} - a^2\right) \psi_n = \zeta_n. \tag{2.5b}$$

As in H78 and Seminara & Hall (1976), the solution can be expressed as

$$\psi_n = \sum_{k=-\infty}^{\infty} \left\{ \alpha_k \sum_{j=0}^{\infty} A_{jkn} E_{jkn}(\gamma_k) + \beta_k \sum_{j=0}^{\infty} B_{jkn} E_{jkn}(a) \right\}, \tag{2.6}$$

where

$$\gamma_k := \sqrt{a^2 + 2\mu + 2ik}, \quad E_{jkn}(\cdot) := \exp(-[\cdot - i(k - n) + |k - n| + 2j]y). \tag{2.7a, b}$$

In addition, the A_{jkn} and B_{jkn} coefficients are scaled so that $A_{0kk} = B_{0kk} = 1$ and the remainder then determined via recurrence relations set out below. Finally the α_k and β_k are found so that the boundary conditions (2.4c) are satisfied. Provided that the real part of γ_k is positive the far-field elements of conditions (2.4c) hold automatically as the $E_{jkn}(\cdot)$ terms decay exponentially in this limit. Thus it is only the two wall constraints that need to be imposed and these become

$$\sum_{k=-\infty}^{\infty} \left\{ \alpha_k \sum_{j=0}^{\infty} A_{jkn} + \beta_k \sum_{j=0}^{\infty} B_{jkn} \right\} = 0 \tag{2.8a}$$

and

$$\sum_{k=-\infty}^{\infty} \left\{ \alpha_k \sum_{j=0}^{\infty} A_{jkn} [\gamma_k - i(k - n) + |k - n| + 2j] + \beta_k \sum_{j=0}^{\infty} B_{jkn} [a - i(k - n) + |k - n| + 2j] \right\} = 0. \tag{2.8b}$$

A non-trivial solution for the unknowns α_k and β_k is required and hence the determinant of coefficients of the infinite set of equations (2.8) must vanish. This condition leads to an eigenrelation for μ in terms of the wavenumber a and Reynolds number R .

The form of solution (2.6) for each harmonic can be interpreted as a formal power series in the variable aR . In particular, the summations over j represent sums over increasing powers of aR , while the summation over k comes from interactions of the harmonics. As the equations are regular in aR these power series are convergent for

all aR with the rate of decay of the terms in the series determining the number of terms that need to be retained in any finite truncation of these infinite series.

The recurrence relation linking the unknowns A_{jkn} and B_{jkn} is rather complicated (see H78) and so, as an aid to programming, several intermediate constants are introduced. The vorticity components ζ_n are expressed in a form analogous to (2.6) with the constants A_{jkn} and B_{jkn} replaced by C_{jkn} and D_{jkn} respectively, so that from (2.5b)

$$C_{jkn} = [(\gamma_k - i(k-n) + |k-n| + 2j)^2 - a^2]A_{jkn}, \quad (2.9a)$$

$$D_{jkn} = [(a - i(k-n) + |k-n| + 2j)^2 - a^2]B_{jkn}, \quad (2.9b)$$

provided that $\mu + ik \neq 0$. If combinations of the various constants are defined by

$$F(j, k, n) := C_{jkn} - 2iA_{jkn}, \quad P(j, k, n) := C_{ijk} + 2iA_{jkn}, \quad (2.10a, b)$$

$$G(j, k, n) := D_{jkn} - 2iB_{jkn}, \quad Q(j, k, n) := D_{ijk} + 2iB_{jkn} \quad (2.10c, d)$$

and the function ϕ given by

$$\phi(j, k, n, \cdot) := [\cdot - i(k-n) + |k-n| + 2j]^2 - a^2 - 2\mu - 2in, \quad (2.10e)$$

then the substitution of the expansions for ψ_n and ζ_n in (2.5a) and a comparison of the coefficients of $E_{jkn}(a)$ and $E_{jkn}(\gamma_k)$ ($E_{jkn}(a)$ and $E_{jkn}(\gamma_k)$ are linearly independent provided, again, that $\mu + ik \neq 0$) gives the required set of recurrence relations. Explicitly they have the form:

if $k \leq n-1$,

$$\phi(j, k, n, \gamma_k)C_{jkn} = iaR \{F(j, k, n-1) + P(j-1, k, n+1)\}, \quad (2.11a)$$

$$\phi(j, k, n, a)D_{jkn} = iaR \{G(j, k, n-1) + Q(j-1, k, n+1)\}; \quad (2.11b)$$

if $k \geq n+1$,

$$\phi(j, k, n, \gamma_k)C_{jkn} = iaR \{F(j-1, k, n-1) + P(j, k, n+1)\}, \quad (2.11c)$$

$$\phi(j, k, n, a)D_{jkn} = iaR \{G(j-1, k, n-1) + Q(j, k, n+1)\} \quad (2.11d)$$

and if $k = n$

$$\phi(j, k, k, \gamma_k)C_{jkk} = iaR \{F(j-1, k, k-1) + P(j-1, k, k+1)\}, \quad (2.11e)$$

$$\phi(j, k, k, a)D_{jkk} = iaR \{G(j-1, k, k-1) + Q(j-1, k, k+1)\}, \quad (2.11f)$$

for $j = 0, 1, 2, \dots$

3. Numerical procedures

For given values of the wavenumber a and Reynolds number R the main computational task is to find a non-trivial finite-dimensional approximate solution to the infinite linear system (2.8). The first step then is to define a reasonable projection from the infinite-dimensional solution space to a finite-dimensional approximation. As the ψ_n are the Fourier coefficients of a smooth periodic function they tend to zero exponentially as $n \rightarrow \infty$. Thus, the truncation imposed here is that $\psi_n(y) = 0$ for $|n| \geq N+1$, which then limits k to the range $-N \leq k \leq N$ in (2.6) and so (2.8) becomes a system of equations for the $4N+2$ unknown coefficients $\alpha_{-N}, \alpha_{-(N-1)}, \dots, \alpha_N, \beta_{-N}, \dots, \beta_N$.

The accuracy of this truncation of the Fourier series is discussed later, but we note here that the location of the neutral modes required values of N in the range 200 to 300.

Those summations appearing in (2.8) to be taken over j were also truncated at a finite value, J . As this sum is analogous to a convergent power series, it was evaluated in reverse, from $j = J$ to $j = 0$ in an attempt to minimize round-off error. Initially J was set at $2N$, but closer examination of the results indicated that J could be safely lowered to 40, for the parameter range considered here, without altering the results. The evaluation of the A_{jkn} and B_{jkn} in these sums was via the recurrence relations (2.11). The fact that k is constant during the j -summation, coupled with the form of the recurrence relations, allowed two-dimensional arrays to be used when evaluating the terms in the j -summations. This resulted in a considerable saving of computer memory, and made the project feasible given the available computing resources.

At the larger values of N , say $N > 200$, it was found that the coefficient matrix in (2.8) developed a block-banded structure. The $(4N + 2) \times (4N + 2)$ coefficient matrix could be partitioned into four $(2N + 1) \times (2N + 1)$ submatrices, where each submatrix had a band width of about 200. The zeros in these matrices were clearly the result of underflow, but it suggested that the coefficient matrix could be approximated by a block-banded matrix with even narrower bands. This idea was confirmed by several numerical experiments and the imposition of this banded structure, using a band width of $N/2$, led to a significant reduction of computer run time without any loss of accuracy in μ .

The determinant of the above block-banded coefficient matrix was then evaluated via an LU -factorization using routines from LAPACK, and an iterative method was used to locate the zeros of the determinant as a function of μ . Several different iteration schemes not requiring function derivatives were tried, but Muller's method proved to be the most efficient. A value of μ was accepted as an eigenvalue of the system if the relative difference in successive predictions for μ was less than 10^{-5} . This usually coincided with a decrease in the size of the determinant of about ten to twelve orders of magnitude and was usually obtained with fewer than ten iterations, depending on the accuracy of the initial guess for μ . As a check on the accuracy of the imposed block banding, the determinant of the full matrix was evaluated at the converged μ and compared with that obtained from the banded matrix. In all cases there was excellent agreement between the two calculations of the determinant. The corresponding eigenvector, that is the corresponding values of $\alpha_{-N}, \alpha_{-(N-1)}, \dots, \alpha_N, \beta_{-N}, \dots, \beta_N$, was then obtained via inverse iteration, which simultaneously provided a check on the accuracy of the eigenvalue μ . The inverse iteration produced an estimate of the smallest eigenvalue of the coefficient matrix (which should be zero) and the rate of convergence to this smallest eigenvalue showed that this 'zero' eigenvalue was eight to ten orders of magnitude smaller than the other eigenvalues of the coefficient matrix. Having found the eigenvector, the disturbance flow field and associated quantities were then reconstructed. Finally we note that it was necessary to use 128-bit arithmetic to obtain the results for the neutral curve. For values of R up to 400, 64-bit arithmetic worked well, but as the number of harmonics increased, round-off error began to contaminate the evaluation of the determinant of the coefficient matrix, making it difficult to locate its zero. Nevertheless, the results with 64-bit arithmetic at $R = 700$ agreed with those obtained using 128-bits but the convergence was much slower with the smaller word-length.

4. Results and discussion

Our main results are summarized in figures 1–4 below: these figures show the behaviour of μ as a function of R for fixed a and illustrate the structure of the neutral curve.† The variation of the imaginary part of μ with R , at the fixed wavenumber $a = 0.3$, for R up to about 200 is given in figure 1(a). These results have the same character as those presented in H78, where it was shown that there are intervals of R where solutions exist which alternate with regions across which no solutions decaying at infinity appear to be possible. At the edges of these intervals $\mu_i \rightarrow 0$ and γ_0 is purely imaginary, as $a^2 + 2\mu_r < 0$, and the solution is only bounded at infinity. To simplify the discussion below, we call the Reynolds number interval between successive bands of solutions with $\mu_i \neq 0$ an S-gap. Thus, as R increases, our results indicate that the length of each S-gap decreases and, simultaneously, the heights of the peaks in figure 1(a) tend to grow towards the value of 0.5. When $\mu_i \neq 0$ discrete eigenvalues correspond to travelling wave disturbances, and as will be shown below, the S-gap will eventually contain standing wave modes.

The behaviour of the real part of μ , μ_r , corresponding to the values of R and a used for figure 1(a), is depicted in figure 1(b). As R increases from zero the disturbances become increasingly more stable although around $R = 80$ this trend shows signs of being arrested. (In H78 equivalent results for a wavenumber $a = 0.15$ indicate that no such levelling off has properly set in by the time $R = 160$.) Moreover, within each solution strip, $\partial\mu_r/\partial R$ is negative. As well as having the same qualitative features as those in H78 our results also agreed quantitatively, at least to graphical accuracy. The procedures adopted in this paper enabled us to take the calculations to much higher R than was possible in H78 and some qualitative changes then begin to appear. First, for R of the order of a few hundred, the growth rates tend to become less negative although at this stage $\partial\mu_r/\partial R$ is still negative on any solution strip and the gap between strips persists. However, once R reaches about 600, $\partial\mu_r/\partial R$ becomes positive over part of the strip until eventually the growth rate is a monotonic increasing function of R , provided that $\mu_i \neq 0$. Continuing to increase R eventually makes $\mu_r > 0$, but we have not shown this on figure 1(b) as there is a subtle change in the solution structure for μ_r very close to zero, and this would not be seen on the scale of this figure.

For $a = 0.3$ our results suggest that the disturbance becomes neutrally stable, with $\mu_r = 0$ and $\mu_i \neq 0$, at $R \approx 780$. But, more importantly, this means that there is a range of Reynolds numbers just below this neutral point where $a^2 + 2\mu_r$ is positive, and this has dramatic effects on the nature of the solutions in the S-gaps just below any such neutral points. (With $a = 0.3$, the relevant range of R is from approximately 772 to 780.) The behaviour of the eigensolutions at infinity is dictated by that of the $E_{000}(\gamma_0)$ term in (2.6). At the edges of the S-gaps $\mu_i \rightarrow 0$, but now, with $a^2 + 2\mu_r > 0$, solutions with the real part of γ_0 negative (see (2.7a)) are possible, and hence an eigenfunction decaying at infinity exists for $\mu_i = 0$, i.e. for standing wave modes. Thus, as found in H78, the S-gaps at Reynolds numbers well below neutral conditions contain a continuous spectrum of standing wave modes which do not decay (spatially) at infinity, as γ_0 is purely imaginary, while in the S-gaps just

† Recently we have examined the linear stability properties of unsteady flow in wide channels using a fully numerical method to determine μ from the governing equations (2.4) with U_B given by the basic oscillatory flow in a channel. The results for μ in the case of a wide channel confirm in detail the results presented in figure 1 of this paper. We intend to present the details of our channel flow stability calculations in a future article.

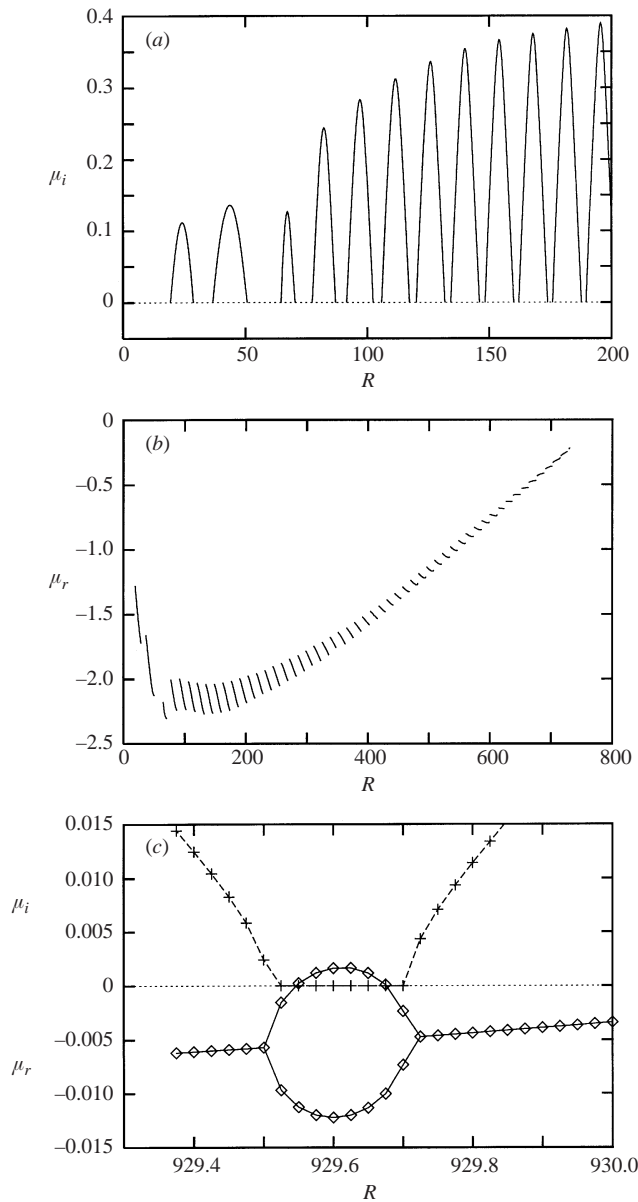


FIGURE 1. (a) Variation of μ_i with Reynolds number R for modes of wavenumber $a = 0.3$. (b) Dependence of μ_r upon R . (c) An example of the behaviour of μ in the vicinity of a region where $\mu_i = 0$. Here $a = 0.25$ and $929.525 < R < 929.7$; the behaviour of μ_r is designated by \diamond and μ_i by $+$.

below neutral conditions there are discrete, standing wave disturbances which decay with increasing distance from the oscillating plate. Further, as indicated below, these discrete standing wave modes emerge from the coalescence of left and right travelling wave perturbations as the phase speed of the travelling waves drops to zero as the Reynolds number is varied, and the edge of an S-gap is approached.

Explicit detail of the above structure is shown in figure 1(c), and to demonstrate that the behaviour is generic, results for a wavenumber of $a = 0.25$ and Reynolds

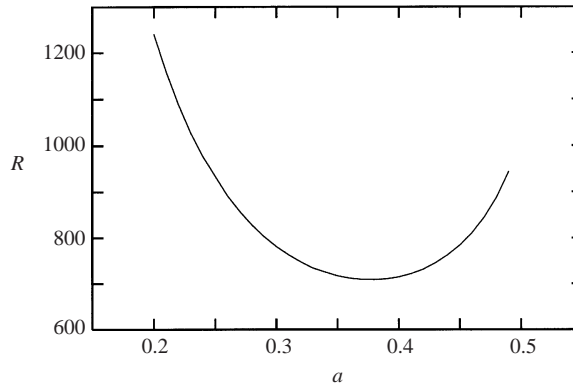


FIGURE 2. Smoothed form of the linear neutral stability curve obtained by interpolation through the neutral points $(a_j, R_N(a_j))$ where $a_{j+1} - a_j = 0.01$.

numbers around 929.6 are presented. The results in figure 1(c) show that μ_i is zero on the S-gap $929.525 < R < 929.7$, and that μ_i is non-zero on either side of this interval. Note that where μ is complex, only the eigenvalues with $\mu_i > 0$ have been plotted in figure 1(c); the $\tilde{\mu}$ eigenvalues have been omitted so the behaviour of growth rate, μ_r , can be seen more easily. The end points of these intervals clearly correspond to a coalescence of the left and right travelling wave modes, i.e. a coalescence of complex conjugate eigenvalues, and while μ_r is now a continuous function of R it must have square-root behaviour at the end points of the $\mu_i = 0$ interval. (Note that the square-root singularity in μ at the ends of the S-gap is masked by the linear interpolation of regularly spaced data points.) However the most remarkable feature of the disturbance in this interval is that the two standing wave solutions, coming from the collision of the complex conjugate eigenvalues, have significantly different growth rates, and that one of the modes is actually unstable on part of this S-gap. At the upper end of this interval the standing wave modes are again both stable and they combine to give stable travelling waves modes as R is increased past the right-hand end of the S-gap. Although not shown in the figure 1(c), these travelling waves eventually become unstable when $R = 930.8$. At this wavenumber, the results obtained indicate that the disturbance does not restabilize as R is increased above 930.8. The occurrence of these regions of unstable stationary modes just below the bulk of the unstable region of parameter space made the precise determination of the neutral curve a difficult process.

The portion of the 'neutral curve' found so far is shown in figure 2. This curve was obtained by interpolation through neutral points $(a_j, R_N(a_j))$ where $a_{j+1} - a_j = 0.01$. A minimum appears to be located at a wavenumber of 0.38 with a Reynolds number of about 708; the corresponding μ_i is 0.15. However, due to the behaviour of the growth rate of the stationary modes, discussed above, this curve is only correct to graphical accuracy; at best this curve defines sufficient conditions for the Stokes layer to be unstable. The precise neutral curve can only be determined by a close examination of the intersection of the region around this curve and the strips where $\mu_i = 0$. Figure 3 shows in detail the structure of the neutral curve around $a = 0.38$. The almost vertical 'spikes' correspond to neutrally stable stationary modes while $\mu_i \neq 0$ on the more gently sloped parts of the curve. These 'spikes' or fingers are in fact smooth, as their lower tip is formed when the upper section of the growth rate curve (for $\mu_i = 0$) has its maximum at $\mu_r = 0$. As the width of the intervals where $\mu_i = 0$ is very small,

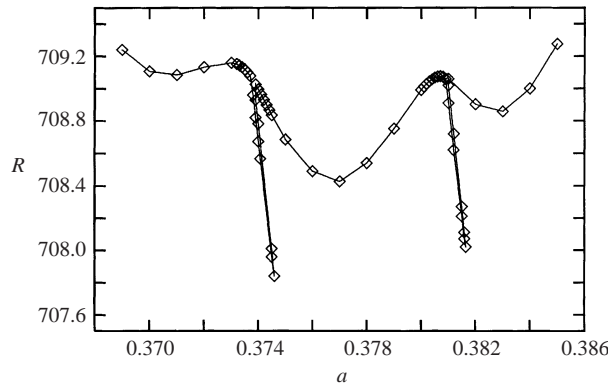


FIGURE 3. Detailed form of the neutral curve in the range $0.368 \leq a \leq 0.385$. The curve is constructed by interpolation between the marked points and shows that in this range the critical disturbance is stationary with $a = a_c = 0.3746$ and $R = R_c = 707.84$.

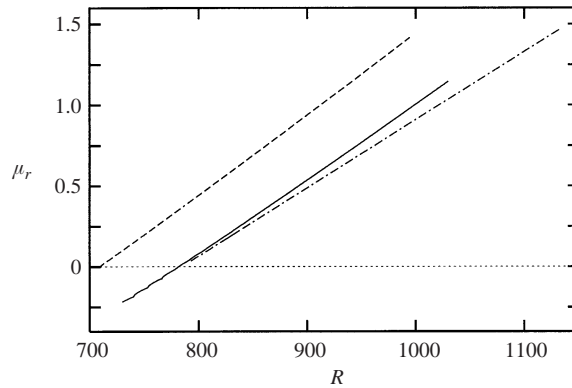


FIGURE 4. The variation of growth rate μ_r as a function of Reynolds number R for modes with wavenumber $a = 0.3$ (solid line), $a = 0.38$ (dashed line) and $a = 0.45$ (chain line).

these fingers will appear sharp when plotted at the scale of figure 3. Figure 3 also shows that the most unstable disturbance is a stationary mode, with $R_c = 707.84$ and $a_c = 0.3746$. Further calculations indicated that around the minimum of the smoothed neutral curve (figure 2) the separation of these fingers was about $\Delta a \approx 0.006$, and hence these spikes occur very regularly. At smaller values of a there is a region where the neutral curve appears to be parallel to the strips of stationary disturbances, and hence there are no fingers off the smoothed curve for this range of wavenumber.

The behaviour of the growth rate, μ_r , for values of R greater than $R_N(a)$ is shown in figure 4. For the three different wavenumbers shown, μ_r increases almost linearly with increasing R . The numerical results for these Reynolds numbers also showed that the dominant harmonics in the wall vorticity moved further away from $n = 0$ as R increased. Allowing for the normalizing condition that $0 \leq \mu_i < 0.5$, these results then suggest that μ_i could also be interpreted as increasing linearly with R , and hence that $\mu \sim \mu_0 R$ for large enough Reynolds numbers. This hypothesis fits naturally with the quasi-steady analysis of Cowley (1987), but as yet there is no asymptotic prediction for μ_0 which could be compared with our numerical estimates. We also note that the maximum growth rate is near $a \approx 0.38$ from our calculations and that this is in reasonable agreement with the results of Cowley (1987).

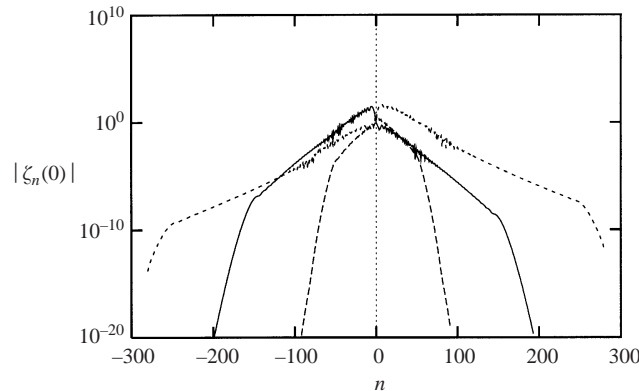


FIGURE 5. Dependence of the magnitude of the wall vorticity component $|\zeta_n(0)|$ upon n for three representative calculations. The innermost curve corresponds to the parameter choices $a = 0.3$, $R = 300$; the solid-line result to $a = 0.27$ and $R = 858$ and the outermost profile to $a = 0.47$ and $R = 843$. Note that in this last case the eventual exponential decay has barely set in even when as many as $N = 280$ harmonics are retained in the computation.

The numerical reliability of these results is best discussed with reference to figure 5, where the distribution of the magnitudes of the wall vorticity components $|\zeta_n(0)|$ versus the harmonic number n for three different calculations is shown. The general shape of these curves is typical of all the results obtained here: the decay of $|\zeta_n(0)|$ with n is initially quite small but at a certain point there is a sudden change and the decay rate accelerates noticeably. Experiments with different truncations, i.e. varying N , of the underlying Fourier series showed that it was essential to include sufficient harmonics in the region of rapid decay of the harmonics in order to guarantee that μ was independent of N . Usually 20 to 30 harmonics in the region of rapid exponential decay of ζ_n were enough to ensure reliable results for μ . The innermost curve on figure 5, for $a = 0.3$ and $R = 300$ shows that a calculation retaining 100 harmonics is easily enough to capture the characteristics of the solution. At the wavenumber/Reynolds number combination $a = 0.27$ and $R = 858$, on the left-hand branch of the neutral curve in figure 2, the distribution of $|\zeta_n(0)|$ widens considerably, but a reliable solution is still possible for $N = 200$. However, at roughly the same R , but now on the right-hand branch, it is observed that the location of the main kink in the curve has moved out to roughly $n = 260$ and thus reliable convergence was just possible within our computational constraints. This illustrates why we were only able to obtain solutions on the right-hand side of figure 2 for values of R just past critical. Further, in the region above the neutral curve, reliable results were achieved provided that N was increased in direct proportion to the increase in aR .

Some indication of the effect of the truncation level N is shown quantitatively in table 1. These results, for $a = 0.3$ and $R = 800$, mimic those in H78 and suggest that under-resolving the disturbance tends to lead to an over-estimate for μ_r . (Notice also that these results confirm that travelling wave modes do become unstable.) It should be anticipated that the convergence in N will be exponential as we are using a spectral method to approximate a periodic function. At numerous stages in our studies calculations akin to those summarized in table 1 were carried out for other values of a and R . In all cases similar behaviours were observed and further tests were conducted in relation to the other truncation parameters: the upper limit J of the j -sums in (2.8) and the bandwidth used in the approximation of the boundary

N	μ
120	(0.684436, 0.574752)
160	(0.119778, 0.367956)
200	(0.081745, 0.350957)
220	(0.081745, 0.350957)
240	(0.081745, 0.350957)

TABLE 1. Variation of the predicted value of μ as a function of the truncation N . This calculation relates to wavenumber $a = 0.3$, Reynolds number $R = 800$, parameter $J = 40$ and the matrix bandwidth set as 201.

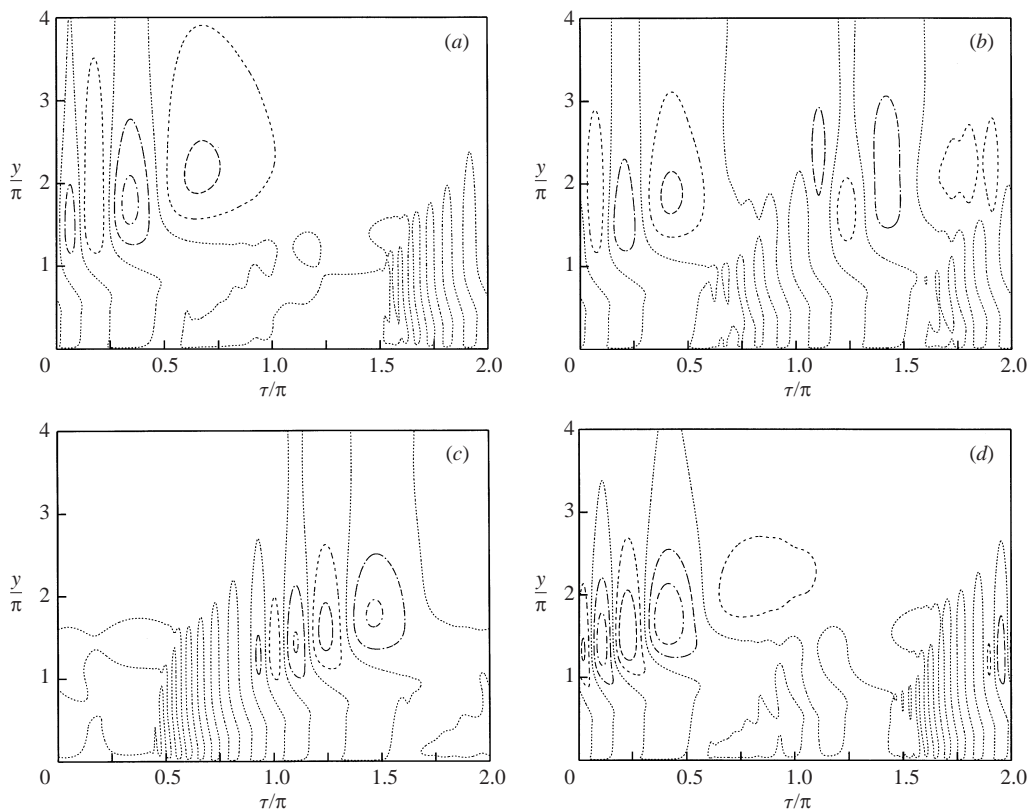


FIGURE 6. Contours of the real part of the disturbance stream function over a period $0 \leq \tau \leq 2\pi$ and the range $0 \leq y \leq 4\pi$. The forms illustrated correspond to the neutral modes at wavenumbers (a) $a = 0.2$, (b) $a = 0.22$, (c) $a = 0.38$ and (d) $a = 0.44$. The interval between successive contours is 250 and the solution has been normalized as described beneath equation (2.7). The zero contour is indicated by the dotted line while positive and negative values of the stream function are designated by dashed and chain lines respectively.

condition matrix. Typical of the results is that for $(a, R) = (0.3, 750)$ and sufficient Fourier resolution ($N > 160$), three significant figures in the value of μ could be obtained for J and bandwidth as small as 20 and 41 respectively.

The structure of ψ_r , the real part of $\psi(y, \tau)$, for neutral modes with $\mu_i > 0$ at wavenumbers of 0.2, 0.22, 0.38 and 0.44 is shown as contour plots of constant $\psi_r(y, \tau)$ in figure 6. The corresponding values of μ_i are 0.165, 0.494, 0.147 and 0.0527

respectively. (The imaginary part of ψ is very similar to the real part and so is not shown.) We note here that for the corresponding solutions with $\mu_i < 0$ the time axis is simply advanced by π in the plots of ψ_r . We also remark that despite the fact that these contour plots are based on a $(2N + 1) \times (4N + 1)$ uniformly gridded data set, the zero contour near the wall $y = 0$ may occasionally be in error. This was observed when two different contouring routines were used on the same data. However, the differences were small and do not affect the features of the flow discussed below.

To begin we note that all four plots share two obvious common features. The first is the result that the maximum stream function occurs close to the edge of the Stokes layer. Given that the basic flow has effectively decayed to zero around $y = 2\pi$, these neutrally stable disturbances extend a significant distance into the region where the basic flow velocity is zero. This structure cannot be completely ascribed to the relatively small values of wavenumber under consideration as a more than doubles from figure 6(a) to 6(d) while the main features of the flow move only fractionally closer to the wall. The other common feature is that the disturbance seems to evolve from a source within the Stokes layer, near $y = \pi/2$ say, which generates a high-frequency oscillation which initially grows in size and propagates along lines $\tau - y = \text{constant}$. As the disturbance grows and moves further from the wall, the frequency of the oscillation slowly decreases, and then the size of the disturbance also begins to decrease. A less obvious feature of these results is that there appear to be two different y values, at a common τ , at which the disturbance has its minimum amplitude. This is best seen in figure 6(d), where for $\tau \approx 3\pi/2$, the disturbance seems to grow simultaneously from near $y = \pi/2$ and from a region very close to the wall. The large values of ψ_r are associated with the source point off the wall, while the regions of negative slope of the $\psi_r = 0$ contour seem to come from the source point near the wall. A plot of the real part of the vorticity field confirmed that there are two regions of high vorticity, of the same sign, propagating away from the wall along two different lines of constant $\tau - y$, with these patches of vorticity gradually merging, and then weakening, as the disturbance moves away from the wall.

The main difference between the four stream function plots appears to be the time at which the disturbance begins its growth phase. For $a = 0.2$ and 0.44 ($\mu_i = 0.165$ and 0.0527), the disturbance begins to increase in size at about $\tau \approx 3\pi/2$; for $a = 0.38$ ($\mu_i = 0.147$) the disturbance grows from $\tau \approx \pi/2$ while for $a = 0.22$ ($\mu_i = 0.494$) it appears that the disturbance grows from both $\pi/2$ and $3\pi/2$. However all the above observations can be broadly summarized by noting that the velocity of the bounding plate is zero at $\tau = \pi/2$ and $3\pi/2$, leading to the general statement that the disturbance begins to grow around the time when the wall velocity is zero. Closer examination of figure 6(c) suggests that even though the biggest disturbance grows from $\tau \approx \pi/2$, there is still some weak perturbation commencing around $\tau \approx 3\pi/2$; equally, figures 6(a) and 6(d) show weak disturbance growth from $\tau \approx \pi/2$ with the main growth beginning around $\tau \approx 3\pi/2$. The extreme case is when there is equal growth from both instants when the wall velocity is zero, and this is approximately illustrated in figure 6(b) where $\mu_i = 0.494$, which is close to 0.5 . As noted earlier, changing the sign of μ_i simply activates the symmetry $\psi(y, \tau) = \tilde{\psi}(y, \tau + \pi)$. But when $\mu_i = 0.5$ the two neutral solutions corresponding to $\mu = \pm 0.5$ are identical, as the Floquet exponents differ by an integer, and hence ψ_r must have period π , meaning that at both instants of zero wall velocity the disturbance growth is the same. Thus for μ_i close to 0.5 it would be expected that the disturbance should have a structure similar to that for $\mu_i = 0.5$, as is confirmed by figure 6(b). Finally we note that $\psi_i(y, \tau) = -\psi_i(y, \tau + \pi)$ when $\mu_i = 0.5$.

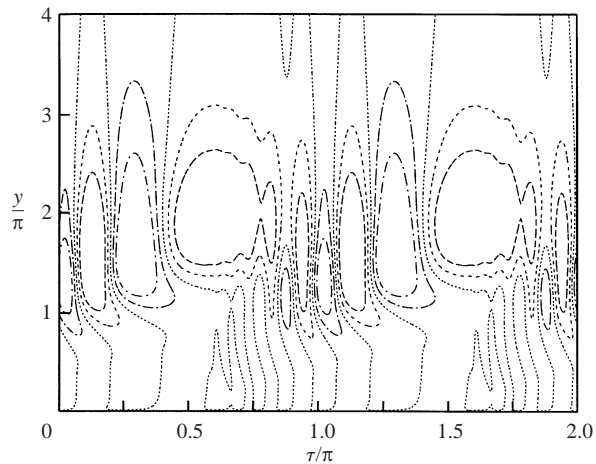


FIGURE 7. Contours of the real part of the disturbance stream function over a period $0 \leq \tau \leq 2\pi$ and the range $0 \leq y \leq 4\pi$ corresponding to the stationary critical mode $R = R_c = 707.84$, $a = a_c = 0.3746$. The line types are as in figure 6 with the interval between successive contours now 500.

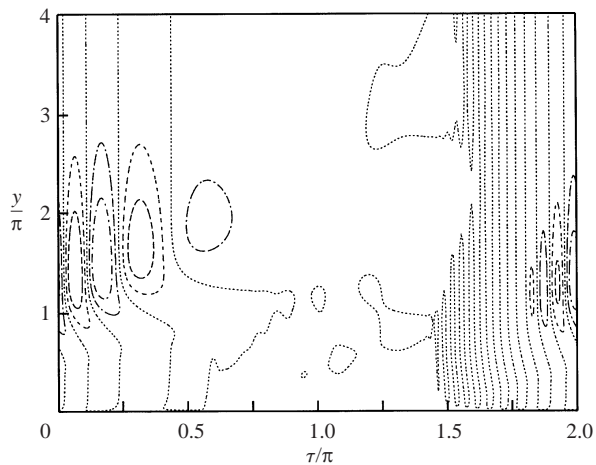


FIGURE 8. Contours of the real part of the disturbance stream function over a period $0 \leq \tau \leq 2\pi$ and the range $0 \leq y \leq 4\pi$ corresponding to the unstable mode $R = 847.5$, $a = 0.38$. The line types are as in figure 6 with the interval between successive contours now 750.

Contours of the real part of the stream function at critical conditions, $a_c = 0.3746$, $R_c = 707.84$ and $\mu = 0$ are shown in figure 7. As both the cases $\mu_i = 0.5$ and $\mu_i = 0$ have the same symmetry properties, figure 6(b) and figure 7 are quite similar but in this latter case the π periodicity in ψ_r is much more accurate. In common with the travelling wave modes, this synchronous disturbance extends well outside the Stokes layer with the main difference between the two types of modes being the strength of the perturbation. All solutions were normalized so that the mean component of vorticity ζ_0 is unity at the wall $y = 0$, but the stream function values for the standing wave solutions are about three times those for the travelling wave modes.

Finally, the contours of the real part of the stream function for the unstable mode with $a = 0.38$ at $R = 847.5$ are shown in figure 8. Here $\mu = (0.675937, 0.148056)$

and the overall features of the structure of this unstable mode are similar to those of the neutral modes: the disturbance begins to grow near the time of zero wall velocity; the frequency of the disturbance decreases as it moves away from the wall and the maximum stream function occurs towards the edge of the Stokes layer. The obvious difference between the structure shown at this higher Reynolds number and the structure of the neutrally stable modes is the much increased local frequency of the disturbance. This increase in frequency is consistent with the suggestion above that $\mu \sim \mu_0 R$ as the Reynolds number increases.

5. Comparison with experimental results and final remarks

From the above discussion of the neutral curve it is clear that any attempt at an experimental determination of critical conditions for the flow above an oscillating flat plate will be rather difficult. While it may be possible to define the critical Reynolds number, the observed structure will be very complicated, as at a Reynolds number 0.1% above critical there are at least three distinct bands of unstable, interacting wavenumbers. Experimentally it may be easier to consider a flow which is oscillating sinusoidally at infinity with the bounding surface stationary, i.e. $U_B \rightarrow U_B - \cos \tau$. In this case the transformation $\zeta \rightarrow \exp(iaR \sin \tau)\zeta$, with a corresponding change in ψ , leaves (2.4) unchanged and so the stability conditions for these two basic flows are the same even though the eigenfunctions will be different. There appear to be only a few experimental investigations into the flow considered here (for example Li 1954), with several other experiments in pipes approximating the semi-infinite Stokes layer. All the experiments summarized by Hino *et al.* (1976) report a critical Reynolds number lower than our result with a value of $R \approx 275$ typical of that quoted. Akhavan *et al.* (1991*a, b*) also give similar values for the critical Reynolds number.

One possible explanation for the above differences is that while we have identified a linear neutral curve with an apparent minimum point there could be another smaller minimum elsewhere in parameter space. In further calculations we have explored a more extensive region and, in particular, investigated wavenumbers as large as $a = 2.5$. However it was found that for given R the growth rate μ_r decreases very rapidly with increasing a which suggests that other neutral modes at Reynolds numbers smaller than those given in figure 3 are unlikely, at least for moderate wavenumbers.

Other possible reasons for the disagreement between our theoretical results and the recorded experimental results may be the effects of finite geometry in the practical apparatus, difficulties in producing an accurate oscillatory flow (as mentioned by Eckmann & Grotberg 1991) or it may be that the instability in the Stokes layer flow is sub-critical. This latter mechanism appears to be unlikely in view of the numerical simulations described by Akhavan *et al.* (1991*b*). Their calculations were performed in the range $R \leq 500$, which is in the region where we predict decaying Floquet modes, and it was shown that the decay rate of small disturbances was larger in full Navier–Stokes simulations than in the runs using linearized equations. A more likely explanation for the disagreement between experiments and the predictions of this work relies on the widely reported observation that the size of the disturbance can vary considerably during one cycle of the basic flow. A global and a local measure of the variation in disturbance size is given below. In figure 9 the magnitude of the enstrophy, $|\int_0^\infty \zeta(y, \tau)^2 dy|$, is plotted as a function of τ for $R = 255, 500$ and approximately 709 with $a = 0.38$. At the largest Reynolds number, which corresponds to neutral conditions for this wavenumber, the maximum magnitude of the enstrophy is about one thousand times the minimum enstrophy, with the variation less at smaller

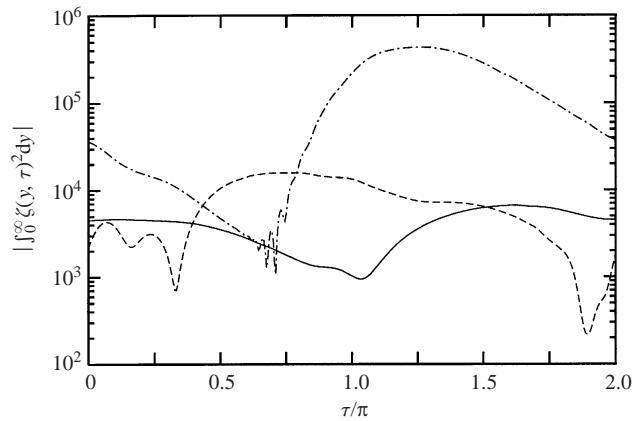


FIGURE 9. Variation of the magnitude of enstrophy $|\int_0^\infty \zeta(y, \tau)^2 dy|$ for wavenumber $a = 0.38$. The solid, dashed and chain lines correspond to $R = 255$, 500 and 709 respectively.

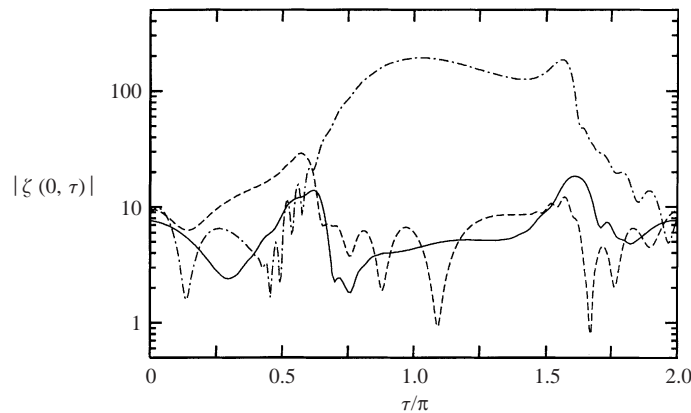


FIGURE 10. Variation of the magnitude of wall vorticity $|\zeta(0, \tau)|$ for wavenumber $a = 0.38$. The solid, dashed and chain lines correspond to $R = 255$, 500 and 709 respectively.

Reynolds numbers. Although not shown, for $R \approx 709$ the real and imaginary parts of the enstrophy oscillate with the same frequency as suggested by the stream function contours in figure 6(c). While indicating that there is significant variation in the size of the disturbance through the cycle, this global measure of the disturbance is not sensitive to local effects in the flow. For comparison, figure 10 shows the magnitude of the wall vorticity, $|\zeta(0, \tau)|$, for the same conditions as in figure 9. At $R = 255$, which is close to the experimental transition Reynolds numbers for bounded flows, the wall vorticity varies by a factor of 10 during one cycle. With $R = 500$ the maximum wall vorticity is 40 times the minimum, while at neutral conditions the ratio of maximum to minimum wall vorticity is about 200. Thus, allowing for a maximum disturbance amplitude of 2% at critical conditions, the background noise in the wall vorticity would need to be less than 0.01% in order for the predicted linear stability to be observed experimentally. These stringent conditions contrast markedly with noise levels of around 2% to 4% reported by Eckmann & Grotberg (1991).

While the linear-theory critical Reynolds number for the instability of flat Stokes layers presented here does not agree with the existing experimental results, the calculated growth rates for the unstable modes do indicate possibilities for further

analytical work. Our limited range of results suggest that for increasing Reynolds numbers a solution with $\mu \sim \mu_0 R + \dots$ may be possible. This hypothesis would lead to, at leading order, an essentially inviscid quasi-steady analysis where critical layer behaviour would be important, and a formal asymptotic calculation as $R \rightarrow \infty$ would then be required.

We are indebted to the referees whose comments led to an improved version of this work. This investigation was conducted while A. P. B. was on study leave at UNSW. He is indebted to the Royal Society of London and the Australian Research Council without whose grants his visit would not have been possible. In addition, he is grateful to the staff and students of New College UNSW and the School of Mathematics for their hospitality.

REFERENCES

- AKHAVAN, R., KAMM, R. D. & SHAPIRO, A. H. 1991*a* An investigation of transition to turbulence in bounded oscillatory Stokes flows. Part 1. Experiments. *J. Fluid Mech.* **225**, 395–422.
- AKHAVAN, R., KAMM, R. D. & SHAPIRO, A. H. 1991*b* An investigation of transition to turbulence in bounded oscillatory Stokes flows. Part 2. Numerical simulations. *J. Fluid Mech.* **225**, 423–444.
- CLAMEN, M. & MINTON, P. 1977 An experimental investigation of flow in an oscillating pipe. *J. Fluid Mech.* **77**, 421–431.
- CLARION, C. & PELISSIER, P. 1975 A theoretical and experimental study of the velocity distribution and transition to turbulence in free oscillatory flow. *J. Fluid Mech.* **70**, 59–79.
- CONRAD, P. W. & CRIMINALE, W. O. 1965 The stability of time-dependent laminar flow: parallel flows. *Z. Angew. Math. Phys.* **16**, 233–254.
- COWLEY, S. J. 1987 High frequency Rayleigh instability analysis of Stokes layers. In *Stability of Time-dependent and Spatially Varying Flows* (ed. D. L. Dwoyer & M. Y. Hussaini), pp. 261–275. Springer.
- DAVIS, S. H. 1976 The stability of time-periodic flows. *Annu. Rev. Fluid Mech.* **8**, 57–74.
- ECKMANN, D. M. & GROTBORG, J. B. 1991 Experiments on transition to turbulence in oscillatory pipe flow. *J. Fluid Mech.* **222**, 329–350.
- HALL, P. 1975 The stability of Poiseuille flow modulated at high frequencies. *Proc. R. Soc. Lond. A* **344**, 453–464.
- HALL, P. 1978 The linear stability of flat Stokes layers. *Proc. R. Soc. Lond. A* **359**, 151–166 (referred to herein as H78).
- HINO, M., SAWAMOTO, M. & TAKASU, S. 1976 Experiments on transition to turbulence in an oscillatory pipe flow. *J. Fluid Mech.* **75**, 193–207.
- VON KERCZEK, C. & DAVIS, S. H. 1974 Linear stability theory of oscillatory Stokes layers. *J. Fluid Mech.* **62**, 753–773.
- LI, H. 1954 Stability of oscillatory laminar flow along a wall. *Beach Erosion Bd, Corps Engrs, USA, Tech. Memo.* 47.
- MERKLI, P. & THOMANN, H. 1975 Transition to turbulence in oscillating pipe flow. *J. Fluid Mech.* **68**, 567–575.
- OBREMSKI, H. J. & MORKOVIN, M. V. 1969 Application of a quasi-steady stability model to periodic boundary-layer flows. *AIAA J.* **7**, 1298–1301.
- SEMINARA, G. & HALL, P. 1976 Centrifugal instability of a Stokes layer. *Proc. R. Soc. Lond. A* **350**, 299–316.
- DE SOUZA, M. O. 1998 Instabilities of rotating and unsteady flows. PhD thesis, Darwin College, University of Cambridge.
- VITTORI, G. & VERZICCO, R. 1998 Direct simulation of transition in an oscillatory boundary layer. *J. Fluid Mech.* **371**, 207–232.
- WU, X. S. & COWLEY, S. J. 1995 On the nonlinear evolution of instability modes in unsteady shear layers—the Stokes layer as a paradigm. *Q. J. Mech. Appl. Maths* **48**, 159–188.